World Academy of Science, Engineering and Technology
International Journal of Mechanical and Mechatronics Engineering
Vol:10, No:10, 2016

Analysis of Vortex-Induced Vibration Characteristics for a Three-Dimensional Flexible Tube

Zhipeng Feng, Huanhuan Qi, Pingchuan Shen, Fenggang Zang, Yixiong Zhang

***Abstract*—**Numerical simulations of vortex-induced vibration of a three-dimensional flexible tube under uniform turbulent flow are calculated when Reynolds number is 1.35×10^4. In order to achieve the vortex-induced vibration, the three-dimensional unsteady, viscous, incompressible Navier-Stokes equation and LES turbulence model are solved with the finite volume approach, the tube is discretized according to the finite element theory, and its dynamic equilibrium equations are solved by the Newmark method. The fluid-tube interaction is realized by utilizing the diffusion-based smooth dynamic mesh method. Considering the vortex-induced vibration system, the variety trends of lift coefficient, drag coefficient, displacement, vertex shedding frequency, phase difference angle of tube are analyzed under different frequency ratios. The nonlinear phenomena of locked-in, phase-switch are captured successfully. Meanwhile, the limit cycle and bifurcation of lift coefficient and displacement are analyzed by using trajectory, phase portrait, and Poincaré sections. The results reveal that: when drag coefficient reaches its minimum value, the transverse amplitude reaches its maximum, and the "lock-in" begins simultaneously. In the range of lock-in, amplitude decreases gradually with increasing of frequency ratio. When lift coefficient reaches its minimum value, the phase difference undergoes a suddenly change from the "out-of-phase" to the "in-phase" mode.

***Keywords*—**Vortex induced vibration, limit cycle, CFD, FEM.

I. Introduction

VORTEX-INDUCED vibration (VIV) occurs in many engineering situations, such as tube bundles in steam generator or heat exchangers, deep sea risers, and so on. Circular cylinder or cylinder bundle is the key components in reactor. The shedding of vortices, alternately and periodically, from a bluff object gives rise to fluctuating lift and drag forces and leads to vibrations and noise; furthermore, it could cause structure failure. Therefore, it is very necessary to further investigate the VIV of 3-D flexible tube.

The practical significance of VIV has led to a large number of fundamental studies, such as turbulence, separation, fluid-structure-interaction, are discussed in many comprehensive reviews [1]. The earlier research on VIV mainly relies on experiment. Many researchers have investigated the flow induced vibrations of elastically mounted rigid tube, such as Feng [2], Griffin [3], Griffin and Ramberg [4], Khalak and Williamson [5], Govardhan and Williamson [6]. The VIV characteristic of cylinder with high mass ratio was conducted by Feng who undertook one of the first comprehensive experimental studies of this problem. Feng's data have only two branches (initial and lower). For the lower mass ratio cylinder system, fairly comprehensive reviews on this VIV problem can be found in the article by Williamson. They found that, at lower Reynolds numbers (3500-10 000), the VIV system has three branches (initial, upper, and lower), a much larger peak amplitude, and a broader synchronization range. The flow field pattern, vortex shedding process, and wake vortex mode are obtained successfully.

Besides experimental study, much progress has been made numerically toward the understanding of the dynamics of VIV. In this complicated problem, a lot of methods were used to solve Navier-Stokes equations, involving computational fluid dynamics (CFD) method [7], [8], Finite element method (FEM) [9], [10], vortex element methods (VEM) [11], [12], time-marching technique [13], and so on. Among these methods, The CFD method is the mostly used. The circular cylinder is generally simulated by an equivalent mass-spring-damper to investigate the dynamics of flow induced cylinder vibration and the influence of cylinder oscillation on flow field. Placzek and Sigrist [14], Mittal and Kumar [15] studied the flow induced vibration characteristics of circular cylinder and wake vortex structure. Evangelinos et al. [8] did a 3-D DNS study (1-DOF) at *Re*=1000 for flexible cylinders. Li et al. [16] used the space-time FEM to investigate the VIV of a two-dimensional elastic mounted circular cylinder under the uniform flow when the Reynolds number is 200. Gabbai and Benaroya [17] reviewed the literature on the mathematical models used to investigate VIV of circular cylinders, and a variety of issues concerning the VIV of circular cylinders were discussed. The strengths and weaknesses of the current state of the understanding of the complex fluid-structure-interaction are discussed in some detail. Sarpkaya [18] made a comprehensive review of the progress made during the past two decades on VIV of circular cylindrical structures subjected to steady uniform flow. The critical elements of the evolution of the ideas, theoretical insights, experimental methods, and numerical models were traced systematically. Though much progress has been made during the past decade, both numerically and experimentally, the complex interaction between structure and fluid is not

Zhipeng Feng is with the Science and Technology on Reactor System Design Technology Laboratory, Nuclear Power Institute of China, Chengdu, Sichuan Province, China (phone: +86-15928515497; e-mail: fengzhipengchn@ 163.com).

Huanhuan Qi is with the Science and Technology on Reactor System Design Technology Laboratory, Nuclear Power Institute of China, Chengdu, Sichuan Province, China (phone: +86-13550368690; e-mail: qihuan73@ 163.com).

Pingchuan Shen is with the Science and Technology on Reactor System Design Technology Laboratory, Nuclear Power Institute of China, Chengdu, Sichuan Province, China (phone: +86-13908068143; e-mail: flily007@ 163.com).

Fenggang Zang and Yixiong Zhang are with the Science and Technology on Reactor System Design Technology Laboratory, Nuclear Power Institute of China, Chengdu, Sichuan Province, China (phone: +86-028-85906144; e-mail: fgzang@ 163.com, zyxnpic@ tom.com).

completely understood yet and remains to be discovered. Meanwhile, VIV of an elastic cylinder is of strongly nonlinear quality [16]. However, there is a few nonlinear analyses. On the other hand, due to the complexity of the flow induced vibration of 3-D flexible tube, current VIV models mostly simplify the 3-D tube to a 2-D elastically mounted rigid tube, thus the elastic distortion is neglected. Therefore, it cannot consider the interaction between elastic distortion of structure and fluid flow. With the equipment process parameters (flow rate, temperature, etc.) becoming higher and higher, it is necessary to construct more accurate physical models to analyze the interactions between fluid and structure as well as their nonlinear response characteristics.

The VIV model based on fully coupled approach combining the CFD and the computational structural dynamics (CSD). The finite volume method, with the dynamic mesh technique to model the motion of tube, is used to compute the flow field, while the FEM is implemented for the tube displacement assessment. The VIV characteristics and nonlinearity of three-dimensional tube under turbulent flow are investigated. Meanwhile, the interaction between tube and fluid is studied numerically. Such an approach is expected to help assessing some vibration for designers.

II. Numerical Model

A. CFD Model

The general conclusion is that even advanced RANS (Reynolds averaged Navier–Stokes) models such as non-linear realizable and RNG types of *k-ε* models severely underestimate the high turbulent kinetic energy levels observed in densely packed tube bundles. The LES results on the fine mesh are comparable to a DNS and experiments and reasonable agreement is still achieved with a coarse mesh [19]. The LES model can obtain satisfactory results in the turbulent flow field which RANS cannot. Thus, the fluid domain is calculated by LES in the present work. The governing equations employed for LES are obtained by filtering the time-dependent Navier-Stokes equations in physical space. Filtering the continuity and momentum equations, one obtains:

$$\frac{\partial \overline{u}_i}{\partial x_i} = 0 \tag{1}$$

$$\frac{\partial \overline{u}_i}{\partial t} + \frac{\partial \overline{u}_i \overline{u}_j}{\partial x_j} = -\frac{1}{\rho}\frac{\partial \overline{p}}{\partial x_i} + \frac{\partial}{\partial x_j}\left(\frac{\mu}{\rho}\frac{\partial \overline{u}_i}{\partial x_j}\right) - \frac{\partial \tau_{ij}}{\partial x_j} \tag{2}$$

where ρ is fluid density, μ is dynamic viscosity, t is time, p is pressure. u_i (i=1,2,3) is velocity components and is Cartesian coordinates. $\overline{p}$ and $\overline{u}_i$ are, respectively, the filtered variable of p and u_i. $\tau_{ij} = \overline{u_i u_j} - \overline{u}_i \overline{u}_j$ is the subgrid-scale stress defined by Algebraic Wall-Modeled LES (WMLES) approach. The WMLES approach combines a modified Smagorinsky model and with a mixing length model and with the wall-damping function. Thereby, WMLES approach can be applied at the same grid resolution to an ever increasing Reynolds number.

B. The Structural Analysis Model

The tube is discretized according to the finite element theory [20] and for each rod a mass matrix (**M**) and a stiffness matrix (**K**) are generated. The Newmark method is used for integrating the dynamics equilibrium equations over time and to analysis transient dynamics.

$$\mathbf{M}\ddot{\mathbf{x}} + \mathbf{C}\dot{\mathbf{x}} + \mathbf{K}\mathbf{x} = \mathbf{F}(t) \tag{3}$$

where **M** and **K** are mass matrix and stiffness matrix respectively, **C** , being the damping matrix, is expressed as a proportional Rayleigh damping $\mathbf{C}=\alpha\mathbf{M}+\beta\mathbf{K}$. $\mathbf{x}$, $\dot{\mathbf{x}}$, and $\ddot{\mathbf{x}}$ are displacement, velocity, and acceleration of node, respectively. The fluid loads coming from the fluid computation by CFD model takes the form of a loading vector on nodes **F(t)**. The initial conditions in velocity and displacement are taken as zero for the whole structures.

C. The Dynamic Mesh Model

Diffusion-based smoothing is used to update a dynamic mesh. For diffusion-based smoothing, the mesh motion is governed by the diffusion equation as in (4):

$$\nabla \cdot (\gamma \nabla \mathbf{u}_s) = 0 \tag{4}$$

where, $\mathbf{u}_s$ is the mesh displacement velocity. On deforming boundaries, the boundary conditions are such that the mesh motion is tangent to the boundary. The diffusion coefficient γ in (4) can be used to control how the boundary motion affects the interior mesh motion and can be a function of the cell volume V, and is of the form $\gamma=1/V^{\alpha}$, and α is the control parameter. Equation (4) is discretized by using finite volume method, and the resulting matrix is solved iteratively. The cell centered solution for the displacement velocity $\mathbf{u}_s$ is interpolated onto the nodes by using inverse distance weighted averaging, and the node positions are updated according to:

$$\mathbf{x}_{new} = \mathbf{x}_{old} + \mathbf{u}_s \Delta t \tag{5}$$

D. The Coupling between Fluid-Structure

Both calculations (fluid and structure dynamics) are using the same time step to implement the fully coupling between fluid and structure by iteration. Data transfer of structure and fluid is achieved via FSI interface. The deformation of fluid domain is defined by displacement of structure obtained via CSD, and the fluid loads are calculated by CFD. Hence, the algorithm is a single loop one:

(1) Solving of displacements and velocity via the structural dynamic equations using the Newmark algorithm and transferring the displacement to dynamic mesh solver.
(2) Updating the fluid domain grid due to the current tube displacement.
(3) Computation of velocity and pressure field and obtaining

fluid forces acting on structure, in addition, transferring them to structure dynamics solver.

(4) Returning to (1) and the calculation proceeds again.

III. The Conditions of the Computation

Tube parameters: tube length L=0.5 m, Outer diameter D=0.01 m, Inner diameter D_i=0.0095 m, Young's modulus E=1×10^5 MPa, Possion's ratio υ=0.3, Density ρ_s=6500 kg/m^3, Damping coefficient α=5.098，β=0.000215. The tube is fixed supported at both the end.

Fluid parameters: The working fluid is water. Density ρ=998.2 kg/m^3, dynamic viscosity μ=0.001003 Pa·s. non-dimensional inflow velocity $U_r=U/(f_nD)$ =0.5~17, where U is the upstream velocity, f_n is the natural frequency of the tube.

Computational domain and boundary condition: the computational domain and mesh is shown in Fig. 1. All the structured grids were generated by using ICEM CFD. In Fig. 1, boundary conditions are a specified fluid inlet for the upstream border (left side in Fig. 1) and a fixed pressure at the downstream one (left side in Fig. 1). Other boundaries are symmetry planes and walls. Tube wall is the fluid-structure interface, and is set as dynamic mesh condition.

Time control parameters: during the calculation, the time step both in structural dynamics computation and fluid dynamics computation is 0.00025 s.

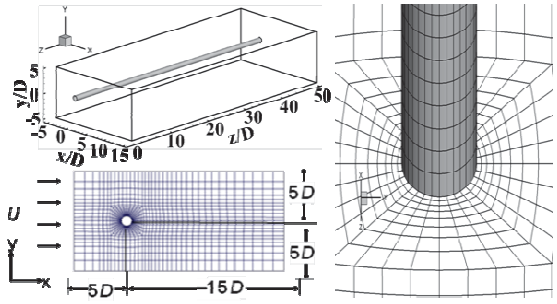

Fig. 1 Schematic of computational domain and mesh

We introduce the following non-dimensional quantities for describing briefly: dimensionless time $t^*=Ut/D$, lift coefficient $C_l=F_l/(0.5\rho AU^2)$, r.m.s (root-mean-square) of the lift coefficient $C_{lRMS}=F_{lRMS}/(0.5\rho AU^2)$, drag coefficient $C_d=F_d/(0.5\rho AU^2)$, mean drag coefficient $\bar{C}_d=\bar{F}_d/(0.5\rho AU^2)$, r.m.s of the drag coefficient $C_{dRMS}=F_{dRMS}/(0.5\rho AU^2)$, streamline displacement x/D, lateral displacement y/D, streamline amplitude $A_x/D=x_{RMS}/D$, lateral amplitude $A_y/D=y_{RMS}/D$, dimensionless vortex shedding frequency $S_t=f_{vs}D/U$, reduced velocity $U_r=U/(f_nD)$, where is the mass per unit length of the tube. ρ_s and ρ are the density of tube and fluid respectively. ζ is the damping ratio. F_{dRMS} and F_{lRMS} are the r.m.s of the drag and lift, respectively. F_d is the mean of drag F_d. x_{RMS} and y_{RMS} are the r.m.s of the streamline displacement and lateral displacement. U is the inflow velocity, D is the diameter of the tube, f_n is the natural frequency of the tube, A is the projective area of computation, t is time.

IV. Investigation of Computational Mesh and Numerical Model

Structured, non-uniform, boundary-fitted grids were generated for the solution domain shown in Fig. 2. All the structured grids used were generated by using ICEM CFD, the grid generation component of ANSYS. The O-type grid is generated around the tube to ensure good quality meshes. The grid expands away from tube boundary in radial-direction with the geometric expansion factor 1.08 within O-block. Away from the O-block, the grid expands with the geometric expansion factor 1.4. Fig. 2 shows the four grids used in present calculation. Table I provides some details of the grids, lift force, drag force, and S_t, including the numbers of nodes on the surface of the tube and in the radial-direction, and the maximum values in the domain of the standard y$^+$. Table I indicates that the four grids have a small standard y+(y^+≈1). It should be noted that, Grid A is the finest grid, Grid B tests the influence of circumference grid nodes, Grid C tests the influence of radial-direction grid nodes, Grid D is the mesh adopted after investigating the influence of grid resolution on flow filed characteristics.

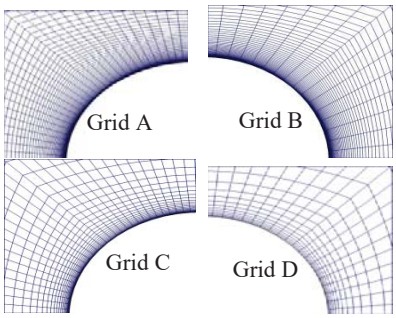

Fig. 2 Computational grid

TABLE I
Details of Grids Used in Mesh-Independence Tests and Their Fluid Force

	N_c	N_r	y+	Cd_{RMS}	St
Grid A	128	65	0.293	0.872	0.248
Grid B	68	65	0.293	0.875	0.229
Grid C	128	33	0.293	0.918	0.229
Grid D	84	17	1.467	0.906	0.229
Norberg [21]	-	-	-	0.99±0.05	0.215±0.005

A mesh refinement study is done to verify the result independence and the accuracy of the method. A uniform flow with Re = 3800 is calculated to assess the performance of the method. The results are compared with the experimental data [21]. The comparison of main parameters is shown in Table I. It is seen that the present result is compared to experimental data and existing models in the literature. That shows the present models are all reasonable. Hence, all computational results are obtained on the grid D mesh. Besides, in order to further validate the numerical model, a case of VIV for a three-dimensional flexible tube is computed and analyzed. Fig. 3 shows the variation of the frequency ratios f_{ex}/f_n, response frequency f_{ex} to natural frequency f_n, and lateral amplitude A_y/D

versus reduced velocity U_r. Meanwhile, the numerical results are compared with the experiment data [22]. As can be shown in Fig. 3, both the amplitude and frequency is compared to experimental data and existing models in the literature. This shows that the present numerical model is reasonable.

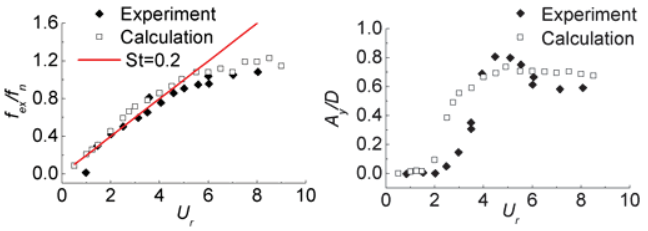

Fig. 3 (a) Tube frequency verse U_r (b) Tube amplitude verse U_r

V. The Results and Discussions

A. Fluid Forces and Vibration Amplitude

The influences of frequency ratio on VIV characteristics of three-dimensional flexible tube are to be discussed by making the inflow velocity fixed and decreasing natural frequency f_n. A summary of several vibration parameters varying with f_n/f_{st} is shown in Fig. 4. Where Fig. 4 (a) shows the effect of frequency ratio f_n/f_{st} on C_{dRMS} (the r.m.s. of drag), C_{dMAX} (the maximum drag), C_{lRMS} (the r.m.s. of lift force coefficient), C_{lMAX} (the maximum drag force coefficient). It is seen that, the maximum and minimum peak value of drag coefficients occurs at f_n/f_{st}=1.25 and f_n/f_{st}=0.56, respectively. The maximum and minimum peak value of lift coefficients occurs at f_n/f_{st}=1.67 and f_n/f_{st}=0.45 respectively. The trends of lateral amplitude A_y/D is shown in Fig. 4 (b). A_y/D reaches its peak value at f_n/f_{st}=0.56. It obviously shows that, the maxima of lateral responses appeared at the minimum drag coefficient, and not the maximum drag coefficient as ordinarily considered. The relationship between f_{vs}/f_{st} and f_n/f_{st} is presented in Fig. 4 (c), where f_{vs} represents the vertex shedding frequency ratio of vibrating tube, f_{st} represents the vortex shedding frequency corresponding to the fixed tube, and f_n/is the natural frequency of flexible tube. The maximum of f_{vs}/f_{st} appears at about f_n/f_{st}=1.25~2, which indicates, in this range of f_n/f_{st}, the interaction effect between tube and fluid flow is the most intense.

When the frequency ratio f_n/f_{st} =0.56~2.5, the lateral amplitude lock-in occurs. Dissimilar to the trends of vibration characteristics versus reduced velocity U_r, the onset of lateral response lock-in occurs at the minimum drag force coefficient (slightly larger than the minimum lift force coefficient) for various frequency ratios. In the peak value range of drag and lift force coefficient and frequency ratio range of lock in, the lateral amplitude is decreasing with the frequency ratio increasing. While in Fig. 4, the onset of lock-in occurs at the reduced velocity U_r corresponding to the maximum lift force coefficient. And the amplitude is constant under lock-in conditions.

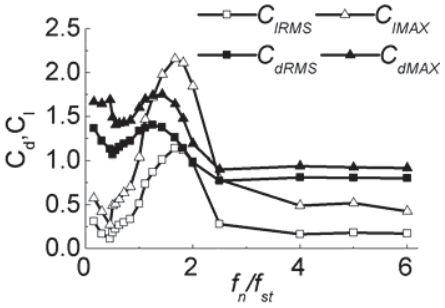

Fig. 4 (a) Force coefficient versus f_n/f_{st}

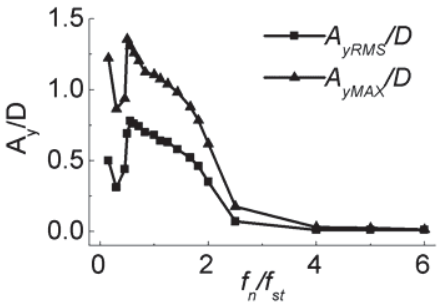

Fig. 4 (b) Lateral amplitude versus f_n/f_{st}

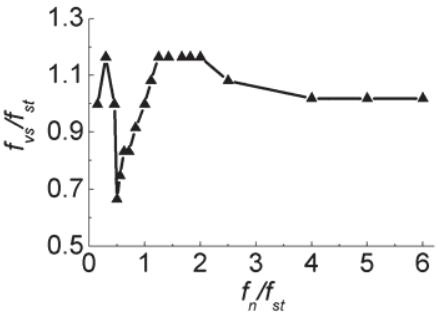

Fig. 4 (c) frequency of vortex shedding versus f_n/f_s

B. Phase difference

The VIV characteristics for three-dimensional flexible tube are very well characterized by plotting the phase ϕ between the lift force and displacement. Fig. 5 shows the phase difference ϕ at different frequency ratios. When the frequency ratio is between 0.45 and 0.5, the phase between the lift force and the lateral displacement undergoes a suddenly change from out-phase to in-phase mode. The jump phenomenon of phase difference is called the ‘‘phase-switch’’, which is a typical nonlinear phenomenon. The phase angle ϕ, found as a function of time by using the Hilbert transform, are shown in Fig. 6. These figures show that, when f_n/f_{st}=0.15, the phase difference is 180°. While in the transition stage, the phase angle “slips” periodically through 360° and its time history becomes disorderly. On the other hand, as f_n/f_{st}≥0.56, the phase difference remains close to 0°. That is to say, phase difference between the lift force coefficient and lateral displacement is in-phase mode.

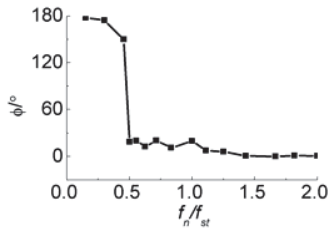

Fig. 5 Phase angle ϕ versus f_n/f_{st}.

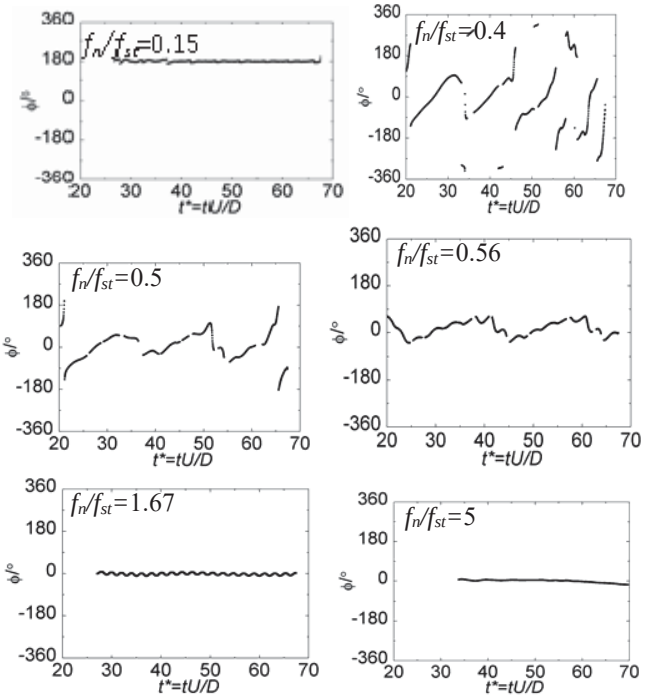

Fig. 6 Time series of phase difference at different f_n/f_{st}

C. Phase Portrait and Limit Cycle

Phase portrait is a very useful tool to analyze dynamics of system. And limit cycle is one of the most important characteristics of nonlinear vibration. The limit cycles of lateral displacement and lift coefficient when f_n/f_{st}=0.15~5 are shown in Figs. 7 and 8, respectively. Fig. 9 shows the Poincaré section of lift coefficient. The C_l' represents the derivative of the lift coefficient and it was calculated by the difference method with second order accurate. The period of the Poincaré map is the vortex shedding period.

When the frequency ratio f_n/f_{st}=0.15 or between $0.56 \le f_n/f_{st} < 2.5$, the shape of the lateral displacement limit cycle is an ellipse. However, the shape of the lift coefficient limit cycle changes from the simple ellipse to the complex geometric figure. Meanwhile, there is only one point in Poincaré section correspondingly. As frequency ratio f_n/f_{st} is any other values, the lift coefficient and lateral displacement curves become very complex. There are a lot of points in Poincaré section which forms a complex situation. However, it is not the chaos motion as it is independent of the initial condition. Thanks to several detailed analyses of limit cycle and Poincaré map of lateral displacement and lift force coefficient at different frequency ratios, it is found that, under turbulent flow, there is no bifurcation of periodic solution for three-dimensional flexible tube within the frequency ratio range from f_n/f_{st}=0.15 to f_n/f_{st}=5.

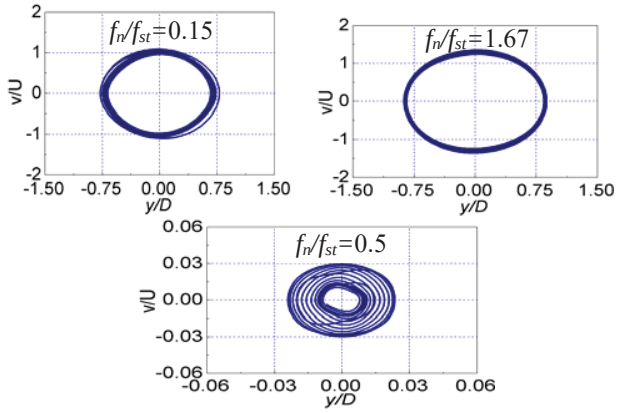

Fig. 7 Limit cycle of the lateral displacement at different f_n/f_{st}

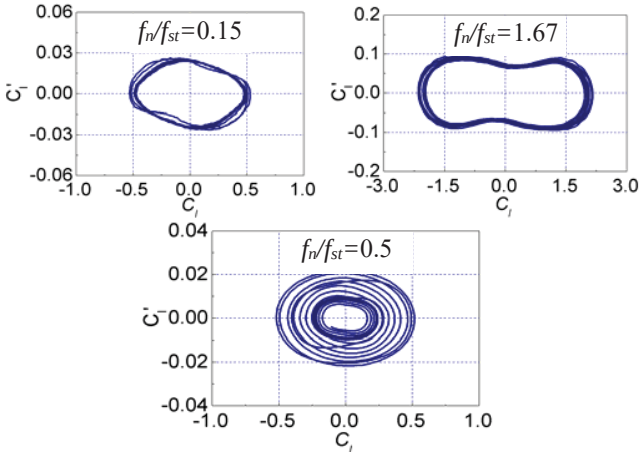

Fig. 8 Limit cycle of the lift coefficient at different f_n/f_{st}

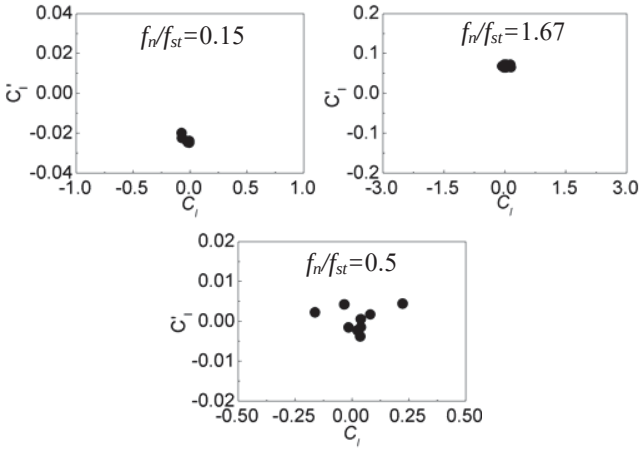

Fig. 9 Poincaré section of the lift coefficient at different f_n/f_{st}

VI. The Analysis of Reynolds Number

In order to discuss the influences of Reynolds number on VIV characteristics for three-dimensional flexible tube, keeping the natural frequency of tube fixed and changing the

inflow velocity, the effects of Re on response are investigated. Where the inflow velocity U=0.5m/s~10.98 m/s and its corresponding Reynolds number range is 5×10^3~1.1×10^5. Fig. 10 shows the vibration parameters at different f_n/f_{st}. In these figures, "U" presents the change of frequency ratio via changing the inflow velocity (therefore changing the Reynolds number and vortex shedding frequency of fixed tube f_{st}). While "f_n" presents the change of frequency ratio via changing the natural frequency f_n. These figures show that, the variation curves of drag force coefficient and amplitude versus frequency ratio on both cases is nearly identical. It reveals that the VIV characteristics of three-dimensional tube manifest are remarkably similar in the Reynolds number range of 5×10^3~1.1×10^5.

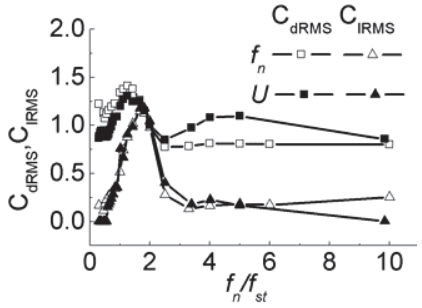

Fig. 10 (a) Force coefficient versus f_n/f_{st}

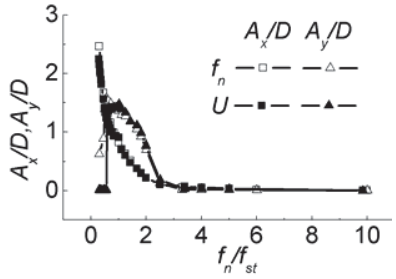

Fig. 10 (b) Amplitude versus f_n/f_{st}

VII. Conclusions

The variation of VIV behavior and nonlinear characteristics for flexible tube versus frequency ratio is investigated by combined CFD and CSD. Conclusions are drawn as follows:

(1) In the peak of drag and lift force coefficient versus frequency ratio, the transverse response lock-in occurs. The amplitude in lock-in decreases with the increase in frequency ratio. The phase angle reaches zero under lock-in, and the dynamic behavior is a periodic motion.

(2) There is no bifurcation of lift coefficient and lateral displacement occurred in three-dimensional flexible tube submitted to uniform turbulent flow when the range of frequent ratio is 0.15~5.

(3) The VIV characteristics of three-dimensional tube manifest are remarkably similar in the Reynolds number range of 5×10^3~1.1×10^5.

References

[1] Goverdhan R, Williamson C H K. Vortex induced vibrations (J). Annual Review Fluid Mechanics, 2004, 36: 413-455.

[2] Feng C C. The measurement of vortex-induced effect in the flow past stationary and oscillating circular cylinder and D-section cylinders (D). Vancouver: University of British Columbia, 1968.

[3] Griffin O M. Vortex-excited cross flow vibrations of a single circular cylinder (J). ASME Journal of Pressure Vessel Technology, 1980, 102: 258-166.

[4] Griffin O M, Ramberg S E. Some recent studies of vortex-excited shedding with application to marine tubulars and risers (J). ASME: Journal of Energy Resources Technology, 1982, 104: 2-13.

[5] Khalak A, Williamson C H K. Motions, forces and mode transitions in vortex-induced vibrations at low mass-damping (J). Journal of Fluids and Structures, 1999, 13(7-8): 813-851.

[6] Govardhan R, Williamson C H K. Modes of vortex formation and frequency response for a freely vibrating cylinder (J). Journal of Fluid Mechanics, 2000, 420: 85-130.

[7] Evangelinos C. Parallel dimulations of vortex-induced vibrations in turbulent flow: linear and non-linear models (D). Providence: Brown University, 1999.

[8] Evangelinos C, Lucor D, Karniadakis G E. DNS-derived force distribution on flexible cylinders subject to vortex-induced vibration (J). Journal of Fluids and Structures, 2000, 14(3): 429-440.

[9] Nomura T. Finite element analysis of vortex-induced vibrations of bluff cylinders (J). Journal of Wind Engineering and Industrial Aerodynamics, 1993, 46-47: 587-594.

[10] Mittal S, Kumar V. Finite element study of vortex-induced cross-flow and in-line oscillations of a circular cylinder (J). International Journal for Numerical Methods in Fluids, 1999, 31: 1087-1120.

[11] Zhou C Y, So R M, Lam K. Vortex-induced vibrations of an elastic circular cylinder (J). Journal of Fluids and Structures, 1999, 13(2): 165-189.

[12] Meneghini J R, Bearman P W. Numerical simulation of high amplitude oscillatory flow about a circular cylinder (J). Journal of Fluids and Structures, 1995, 9 (4): 435-455.

[13] Jadic I, So R M C, Mignolet P. Analysis of fluid-structure interactions using a time-marching technique (J). Journal of Fluids and Structures, 1998, 12(6): 631-654.

[14] Placzek A, Sigrist J F. Numerical simulation of an oscillating cylinder in a cross-flow at low Reynolds number: Forced and free oscillations (J). Computers & Fluids, 2009, 38:80-100.

[15] Mittal S, Kumar V. Flow-induced vibration of a light circular cylinder at Reynolds numbers 103 to 104 (J). Journal of Sound and Vibration, 2001, 245(5): 923-946.

[16] Li T, Zhang J Y, Zhang W H. Nonlinear characteristics of vortex-induced vibration at low Reynolds number (J). Commun Nonlinear Sci Numer Simulat, 2011, 16: 2753-2771.

[17] Gabbai R D, Benaroya H. An overview of modeling and experiments of vortex-induced vibration of circular cylinders (J). Journal of Sound and Vibration, 2005, 282: 575-616.

[18] Sarpkaya T. A critical review of the intrinsic nature of vortex-induced vibrations(J). Journal of Fluids and Structures, 2004, 19: 389-447.

[19] Benhamadouche S, Laurence D. LES, coarse LES, and transient RANS comparisons on the flow across a tube bundle (J). International Journal of Heat and Fluid Flow, 2003, 24: 470-479.

[20] WANG X C. The finite element method (M). Beijing: Tsinghua University Press, 2003: 468-495.

[21] Norberg C. Fluctuating lift on a circular cylinder: review and new measurements (J). Journal of Fluids and Structures, 2003, 17: 57-96.

[22] Schowalter D, Ghosh I, Kim S E, Haidari A. Unit-tests based validation and verification of numerical procedure to predict vortex-induced motion (C). Proceedings of OMAE2006, 25th International Conference on Offshore Mechanics and Arctic Engineering, Hamburg, Germany, 2006: 184-187.